Influence of temperature on crater and ejecta size following hypervelocity impact of aluminum alloy spheres on thick aluminum alloy targets

Masahiro Nishida*, Koichi Hayashi, Junichi Nakagawa and Yoshitaka Ito

Department of Mechanical Engineering, Nagoya Institute of Technology,
Gokiso-cho, Showa-ku, Nagoya 466-8555, Japan

* Corresponding author. Tel.: +81- (0) 52-735-5349; fax: +81-(0)52-735-5342.
E-mail address: nishida.masahiro@nitech.ac.jp (M. Nishida).

Keywords: Hypervelocity impact, Temperature effect, Thick target, Ejecta fragment, Cratering

Abstract.

The influence of temperature on crater shape and ejecta fragment size in thick aluminum alloy targets was investigated for impact velocities ranging from approximately 0.9 to 3.5 km/s using a two-stage light-gas gun. The diameter, depth, and volume of the crater increased with increasing temperature. Observation of the witness plates showed that the scatter diameters and angles of the ejecta were slightly smaller at high temperatures than at low and room temperatures. Temperature affected the size and mass of ejecta fragments collected from the chamber only when the impact velocity was 1.5 km/s (the velocity at which the projectile fragmentation started). As the temperature increased, its influence on the mass of ejecta fragments decreased. Temperature affected the length and the axial ratios of ejecta fragments only at an impact velocity of 1.5 km/s. Regardless of the temperature and impact velocity, the axial ratios, *c/a,* were less than 0.6.

1. Introduction

Space debris has no useful purpose and often strikes spacecraft and space stations at velocities over several kilometers per second (hypervelocity impact). The International Space Station employs shields such as the Whipple bumper and the stuffed Whipple bumper to protect itself from space debris. Debris clouds are formed when high-velocity projectiles perforate these bumpers, which consist of thin plates. Many studies have been conducted on the formation and structure of debris clouds. Many researchers have suggested various improvements to bumpers, which have resulted in an increase in bumper strength, reduction in the amount of debris generated, decrease in the spread area of debris, etc.

Projectiles with low kinetic energy—those with a small size or low velocity—do not perforate the bumpers and outer surfaces of spacecraft and space stations; instead, they form craters on these surfaces. In such cases, fragments from the target surface are ejected, and the projectile fragments are widely scattered. These fragments become new debris, as pointed out by Murr and coworkers in 2004 [1]. They studied the hypervelocity impacts of projectiles on thick targets and examined the crater formation and impact fragmentation of projectiles both experimentally and numerically [2]. Takayama's group at Tohoku University carried out impact experiments in which cylindrical projectiles 10 mm in diameter and 10 mm in thickness and made of aluminum alloy 2017-T4 struck thick targets made of aluminum alloy 2017-T4. The group examined the carefully recorded images of ejecta clouds in detail [3]. They also captured ejecta fragments utilizing the soft recovery technique, using a silicone rubber sheet 10 mm in thickness, and studied the number and size of ejecta to clarify the ejecta composition when high carbon-chromium bearing steel (SUJ-2) projectiles struck aluminum alloy 2017-T4 plates and, on the other hand, when the aluminum alloy 2017-T4 projectiles struck SUJ-2 plates [4]. Current research has been shedding light on how ejecta are formed, but in addition to this, the international standardization of test procedures is being promoted for the evaluation of spacecraft material ejecta [5]. Several studies have been conducted on the ease and precision of techniques to evaluate ejecta [6, 7].

In planetary science, there have been some studies on ejecta size and ejecta mass of planetary materials (i.e., brittle and/or porous materials) [8, 9]. Numerous studies have also analyzed the impact of projectiles on thin plates in order to statistically understand the mechanism of dynamic fragmentation. For example, in 1998 Grady and Kipp [10] examined the fragmentation of debris clouds. Piekutwski [11] examined fragment diameters when spherical projectiles struck thin-sheet targets. De Chant [12] simulated fragment size for metal plates. However, few studies have been conducted on crater shape and ejecta fragment size when ductile projectiles strike thick ductile targets. In addition, the temperature of spacecraft and artificial satellites in low Earth orbit (LEO) varies from approximately 100 K to 400 K. However, no studies have ever investigated the influence of temperature on both crater shape and ejecta fragment size, although a few studies have investigated the influence of target temperature on crater shape alone [13], and several studies have analyzed the influence of temperature on the perforation behavior of projectiles impacting thin plates (e.g., Corbett [14, 15] analyzed the hole diameter of 6061-T6 Al plates; Numata et al. analyzed AL5052-H34 and AL2024-T3 plates [16] and CFRP plates [17]; Francesconi et al. [18] analyzed aluminum bumpers; Wells [19] analyzed coated thermoplastic films).

In this study, we investigated the effects of temperature on crater shape and ejecta fragment size when aluminum alloy spheres, accelerated by a two-stage light-gas gun, impact thick aluminum alloy targets at velocities ranging from 0.9 to 3.5 km/s. The crater diameter and crater depth of the targets were measured after impact. The size and mass of ejecta fragments collected from the test chamber were also examined in detail. The witness plates were observed after the experiments.

2. Experimental Setup

We used thick targets (120-mm diameter, 30-mm/40-mm thickness, depending on impact velocity) made of aluminum alloy 6061-T6 with two cut-off surfaces, as shown in Fig. 1; the creation of cut-off surfaces resulted in an increase in contact area between the targets and the heater/cooler, which facilitated more efficient heating/cooling of the targets. Cartridge heaters were used as the heating device, and liquid nitrogen, which was circulated around the external surface of the chamber, was used as the cooling medium. The temperature of the targets immediately before impact was measured using a thermocouple. The target temperatures were as follows: high temperatures ranging from +194 to +210°C, room temperatures ranging from +14 to +26°C, and low temperatures ranging from -136 to -157°C.

We employed aluminum alloy (2017-T4) projectiles with a diameter of 14.2 mm and a weight of 4.17 g. The spherical projectiles were accelerated using a two-stage light-gas gun and made to strike the thick aluminum alloy targets. The impact velocity of each projectile was determined on the basis of the time it took to travel between two sets of laser sensors immediately before collision with the thick aluminum alloy targets. The impact velocities ranged from 0.9 to 3.5 km/s.

In order to examine the effects of the mechanical properties of the alloys on ejecta scattering and impact fragmentation of the projectiles, a witness plate made of aluminum alloy (130 mm × 230 mm), with a hole 20.5 mm in diameter through which the projectiles could pass, was placed 45 mm from each target, as shown in Fig. 2. After the experiments, the crater shape was measured, and ejecta was collected from the test chamber. Table 1 lists the values of the tensile strength, yield stress, and elongation of aluminum alloy 6061-T6, obtained by performing static tests at high, room, and low temperatures [19], as well as the measured Vickers hardness values.

3. Results and Discussion

3.1 Crater shape

Figure 3 shows the effect of impact velocity in photographs of craters impacted at high temperatures. The crater size increased, and the crater lip that turned outward developed as impact velocity increased. When the impact velocity reached 3.47 km/s, the crater lip appeared broken. It seems that the broken crater lip became ejecta fragments due to high impact pressure. The crater wall is roughened

Figure 4 shows the effect of temperature on crater shapes when impacted at a velocity of approximately 2.5 km/s. The craters created at high temperatures developed long lips that turned outward. The crater lips created at low temperatures were not long; they appeared broken, and the craters' edges were rough. We measured crater shape using a contour recorder (Tokyo Seimitsu Co., Ltd., Contourrecord 600B). Figures 5(a)–(d) show

a comparison of the crater shapes at different target temperatures for each impact velocity. At an impact velocity of approximately 1 km/s, as shown in Fig. 5(a), the depth at high temperatures was clearly greater than at low and room temperatures. The diameter at high, low, and room temperatures was almost the same. At this impact velocity, it seems that the projectile only made a dent in target. When the impact velocity was approximately 1.5 km/s in Fig. 5(b), the diameter and depth of the crater increased with increasing temperature. At an impact velocity of approximately 2–2.5 km/s, as shown in Figs. 5(c) and (d), the crater shape at all temperatures was semispherical. At an impact velocity of approximately 3.5 km/s, as in Fig. 5(e), the crater shape at high temperatures was oval rather than semispherical.

Figures 6(a) and (b) show the crater diameter and crater depth normalized by the projectile diameter for all experiments. The crater diameter and depth were defined assuming an undisturbed surface, as shown in Fig. 7. Here, the measurement error of the crater depth for the same crater was within approximately 2 % and the repeatability error of the same cross-section (the instrument error) was within approximately 0.2 %. Therefore, the following changes in depth and diameter are discernible. Predictably, the normalized crater diameter and depth increased with increasing impact velocity. The temperature only slightly affected the crater diameter, resulting in a change of ±4–6%; on the other hand, the temperature affected the crater depth, resulting in a change of ±13–15%. This tendency agrees with the prediction made using the JSC equation [21], which explains the hardness effect on the crater depth:

$$\frac{P_c}{d_p} = 5.24\, d_p^{\,1/18} H_B^{\,-0.25} \left(\frac{\rho_p}{\rho_t} \right)^{0.5} \left(\frac{V}{c_B} \right)^{2/3} \tag{1}$$

Here, P_c is the crater depth, d_p is the projectile diameter, H_B is the Brinell hardness of the target, ρ_p is the projectile density, ρ_t is the target density, V is the impact velocity, and c_B is the velocity of the bar wave of the target. We considered the effects of temperature on crater depth quantitatively. Because the relationship between Brinell hardness number and Vickers hardness number had an almost one-to-one correspondence (a linear function passing through the origin) and the Vickers hardness of target materials could be measured easily, we considered the effects using Vickers hardness. The analysis using Brinell hardness was almost the same as that using Vickers hardness when we used the change rate. According to eq. (1), because changes in temperature caused the Vickers hardness to change ±10–15%, as shown in Table 1, the crater depth is expected to change only ±3–4% of the change in hardness. However, this prediction does not agree with the experimental results, which show a change of ±13–15%, as seen in Fig. 6 (b).

Watts and Atkinson proposed an equation to determine the penetration depth of projectiles into infinite targets using the -1/3 power of targets' yield stress instead of hardness [22, 23]. This equation does not explain the experimental results in Fig. 6(b), because the yield stress changed +20% and -60% of the temperature change, as shown in Table 1. Lieblein et al. [24] studied the effect of elevated temperature (700K) on crater depth when aluminum projectiles struck aluminum targets. They showed that the experimental data could be explained using a function based on the elastic modulus and Brinell hardness. It seems that the elastic modulus, the hardness and the yield stress are important for the crater depth. However, because the values of the elastic modulus, the hardness and the yield stress change in a mutually dependent manner, it is difficult to

examine the effects of each factor separately.

Next, the crater volume was examined. As shown in Figs. 3, 4, and 5, the crater shape is not semi-spherical and the surface of crater wall is roughened. We measured crater volume with high accuracy by pouring ethanol into the craters; the surface tension of ethanol, approximately 20 mN/m, is lower than that of water, approximately 75 mN/m. Here, the crater volume was defined as the volume of the dent below the undisturbed surface, as shown in Fig. 7. Figure 8 shows the crater volume normalized by the projectile volume. Under the impact velocity conditions of the present experiment, the normalized crater volume was almost directly proportional to the impact velocity, regardless of temperature. At impact velocities of 2.5 km/s and 3.5 km/s, an increase in temperature affected the crater volume, resulting in a change of 20%, and a drop in temperature resulted in a change of 10%. Even though the rise and fall of the target temperature were almost the same, the rise and fall of the target hardness were not the same and the changes in crater volume induced by the temperature fluctuations were not the same. Here, because the measurement error of crater volume was within approximately 4 %, the above changes were discernible.

In 1964, Piacesi et al. [25] studied the effect of elevated temperature (180ºC, 190 ºC and 260 ºC) on crater volume using aluminum alloys 2017 and 7075 targets and 1/4-inch diameter aluminum spheres. They concluded that the crater volume was dependent on the -0.396 power of the yield strength. If you look at the figure, most results of elevated temperature appear to be a little above the line showing the -0.396 power of the yield strength. It seems that it is difficult for the results of elevated temperature to be explained only by the yield strength. Because there is a strong relation between the yield stress and the hardness of materials, it is difficult for the results of elevated temperature to be explained by either only the yield strength or only the hardness. This result supports our own results. We should consider other factors in addition to the hardness or the yield stress of the targets. In 1960, Allison et al. [26] studied the effect of temperature (77K to 700K) on hypervelocity cratering using lead, copper, zinc and cadmium targets and steel fragment projectiles. They drew a figure which shows crater volume versus temperature normalized by melting points. By inferring from the author's results and others' results using different materials under different temperature conditions, there is a high possibility that the difference between the melting point and the initial temperature of the targets affected the experimental results. It seems that the difference between the melting point and the initial temperature of the targets produced the result that the changes in crater volume induced by the temperature fluctuations were different. The target surface whitened when the impact velocity was high. It seems that part of the target and/or projectile melted and vaporized at the moment of impact.

3.2 Observation of indentation in witness plates

We observed the witness plates after the experiments. Figure 9 shows the effects of impact velocity in photographs of the witness plates at high temperature. When the impact velocity was 1.04 km/s, we observed a few indentations in the witness plate. The projectile was distorted, and the edge of the projectile was only slightly fragmented, as shown in Fig. 15. When the impact velocity was 2.14 km/s, we observed many indentations. Few indentations were observed in the center of the witness plate, near the hole through which

the projectile passed. Outside the undamaged circular area, we could see a ring of indentations caused by the impact of ejecta. We deduced that the indentations were induced by ejecta fragments from the targets, because the indentations were shallow and small. In addition, we observed small radial indentations outside of the ring. We can more clearly observe the ejecta ring and small radial indentations at an impact velocity of 2.67 km/s, as shown in Fig. 9(c).

Figure 9(c) and Figs. 10(a) and (b) show the effects of temperature in photographs of the witness plates at an impact velocity of approximately 2.5 km/s. The features of the indentations in the witness plates were almost the same at every temperature. The undamaged circular area, ejecta ring, and radial indentations were observed regardless of the temperature. It appears that the diameter of the ejecta ring at high temperatures was slightly smaller than at low and room temperatures, and the ejecta ring was whiter at high temperatures than at low and room temperatures.

Next, we measured the inner diameter of the ejecta ring, D_{ej}, as shown in Fig. 11. In Fig. 12, the vertical axis shows the inner diameter of the ejecta ring normalized by the projectile diameter. For each temperature, the normalized diameter of the ejecta ring decreased gradually as impact velocity increased. The normalized ejecta ring diameter was roughly proportional to the impact velocity to the -0.5th power. At impact velocities of less than 2 km/s, the ring diameter was slightly smaller at high temperatures than at low and room temperatures. The ring diameter at low temperatures was almost the same as it was at room temperature. Myers et al. [27] reported that the variance between the heated bumper data and the room temperature hole diameter models was most prominent at 2 to 4 km/s when the projectile perforated thin plates. The variance appeared to decrease with increasing velocity. The trend shown by Myers et al. was similar to the results of eject ring diameter.

We examined the scatter angle of the ejecta, ϕ, defined in Fig. 13. We employed the following equation using the ejecta ring diameter, D_{ej}, and the final crater diameter, d_c.

$$\phi = \tan^{-1}\left(\frac{D_{ej} - d_c}{2 \times 45}\right) \tag{2}$$

Figure 14 shows that, for each temperature, the scatter angle decreased gradually as impact velocity increased. For all impact velocities, the scatter angle was clearly smaller at high temperatures than at low and room temperatures. At high temperature, the hardness of the target was low. It seems that the hardness of the target was important in this case. It is believed that the hardness of the targets affected wall angles of transient craters during projectile penetration (not final craters) and the scatter angle became smaller.

3.3 Ejecta collected from test chamber

All the ejecta fragments from the targets were collected from the test chamber after impact experiments, along with all the projectile fragments. The collected ejecta are shown in Fig. 15. An impact velocity of 1 km/s yielded deformed projectiles without much breakup or fragmenting. At low temperatures, as shown in Fig. 15(L-1), two large fragments could be united, and the resulting shape was almost the same as the shape of projectiles collected at both room and high temperatures. Predictably, the projectiles were more fragmented

with increased impact velocity. When the impact velocity was under 2.5 km/s, significantly larger particles were visible. At impact velocities of 2.5 km/s and 3.5 km/s, many small ejecta (under 50 mg) were also collected, as shown in Figs. 15 (H-4), (R-4), (L-4), (H-5), (R-5), and (L-5). It appears that, for each impact velocity, the ejecta were slightly larger at high and room temperatures than at low temperatures. Contrary to our expectations, temperature did not obviously affect the outward appearance of ejecta.

Figures 16(a)–(d) show the cumulative number distribution of ejecta fragment mass, which means the number of ejecta fragments with a mass greater than the mass of ejecta fragments on the horizontal axis, on a double logarithmic scale. The maximum ejecta mass decreased with increasing impact velocity. At high temperatures, larger fragments, indicated in the figures by black squares, were collected for impact velocities over 2 km/s. For example, when the impact velocity was 2.5 km/s, as in Fig. 16(b), particles around 1 g were collected at high and room temperatures, whereas particles around 0.5 g were collected at low temperatures. It was found that projectiles fragmented to some extent at an impact velocity of 2.5 km/s, which can be explained by the fact that the initial mass of projectiles was 4.17 g. The cumulative number distribution of ejecta fragment mass, in particular the smaller ejecta fragment mass, was almost the same when impact velocity was over 2 km/s.

Next, we measured the size (length a, width b, thickness c) of ejecta, as defined in Fig. 17. Figures 18(a)–(d) show the cumulative number distribution of ejecta fragment length, a. Here, the measurement error of ejecta was within approximately 4 %. At the impact velocity of 1.5 km/s, the temperature had a slight impact on ejecta fragment length. At room temperature, the small ejecta were collected more than at high and low temperatures. Because the elongation at break at room temperature was the smallest, there is a possibility that the elongation at break was important for the ejecta at this impact velocity. Once impact velocity exceeded 2 km/s, the influence of temperature on ejecta fragment length decreased with increasing impact velocity. A possible explanation is that the kinetic energy of projectiles over 2 km/s eclipses the initial heating up and cooling down energy. The cumulative number changed at an increasing rate: approximately 6 mm at the an impact velocity of 1.5 km/s and approximately 6 and 10 mm at impact velocities of 2 km/s and 2.5 km/s. When the impact velocity was 3.5 km/s, the change in the increasing rate was not clearly observed at 10 mm and the change in the increasing rate was only observed at approximately 7 mm. We hypothesized that the ejecta fragments larger than 6 mm at 1.5 km/s/10 mm at 2 km/s and 2.5 km/s came mainly from projectile fragmentation, while those smaller than 6 mm/10 mm came mainly from the targets.

The axial ratios, b/a, are shown in Fig. 19. The vertical axes in Fig. 19 represent the cumulative number distribution of the axial ratios of ejecta fragments, which means the number of ejecta fragments with an axial ratio greater than the axial ratio of ejecta fragments in the horizontal axis. At an impact velocity of 1.5 km/s, the temperature only slightly affected the tendency of b/a. Regardless of the temperature, the tendency of b/a remained more or less constant over 2 km/s.

The axial ratios, c/a, are shown in Fig. 20. A c/a value close to 1 indicates that the ejecta are thick, and a c/a value close to 0 indicates that they are thin. The temperature affected the tendency of c/a at each impact velocity, in contrast to b/a. There is not any clear tendency of c/a in regard to temperature. We expected that c/a would be thinner at high temperatures because of the elongation of the target. However, the results were to

the contrary. Regardless of temperature and impact velocity, the value of *c*/*a* fluctuated below 0.6. When the impact velocity was over 2 km/s, the change in the material properties of target, such as the hardness, elongation at break and the elastic modulus, was less important for the mass and size of ejecta.

4. Summary

Compared to the measurement errors, temperature significantly affected crater depth and crater volume, and only slightly affected crater diameter. The trend of the experimental results was similar to those of temperature effects reported by Lieblein et al. [24], Piacesi et al.[25] and Allison et al. [26]. The scatter diameter and scatter angle of ejecta at high temperatures were slightly smaller than at low and room temperatures. At the impact velocity at which the projectile fragmentation started (1.5 km/s), the mass of ejecta fragments collected from the test chamber at low temperatures was slightly smaller than the mass collected at high and room temperatures. Temperature affected the length and the axial ratios of ejecta fragments only at an impact velocity of 1.5 km/s. The distribution of the axial ratios, *b/a* and *c*/*a*, of ejecta fragments remained more or less constant at impact velocities over 2 km/s. The trend of temperature effects was similar to that of Myers et al. [27] showing that the variance decreases with increasing velocity. Regardless of temperature and impact velocity, the value of c/*a* fluctuated below 0.6.

Acknowledgments

The authors are greatly indebted to Associate Professor Yasuhiro Yoshino of Iwate University and Mr. Kazuto Sato of Fujimi Incorporated for their help with the Vickers hardness measurements at low and high temperatures. This work was supported in part by a Grant-in-Aid for Scientific Research (C), KAKENHI (22560078), from the Japan Society for the Promotion of Science (JSPS).

References

[1] V.S. Hernandes, L.E. Murr, I.A. Anchondo, Experimental observations and computer simulations for metallic projectile fragmentation and impact crater development in thick metal targets, Int. J. Impact Eng. 32 (2006) 1981–1999.

[2] O.L. Valerio-Flores, L.E. Murr, V.S. Hernandez, S.A. Quinodes, Observations and simulations of the low velocity-to-hypervelocity impact crater transition for a range of penetrator densities into thick aluminum targets, J. Mat. Sci. 39 (2004) 6271–6289.

[3] D. Numata, T. Kikuchi, M. Sun, K. Kaiho, K. Takayama, Experiment study of ejecta composition in hypervelocity impact using ballistic range, Proc. of Symp. Shock Waves in Japan, (2007) 221-222.

[4] D. Numata, T. Kikuchi, M. Sun, K. Kaiho, K. Takayama, Experiment study of ejecta composition in impact phenomenon, Proc. 26th Int. Symp. Shock Waves, (2007) Part X.

[5] Space Systems-Test procedures to evaluate spacecraft material ejecta upon hypervelocity impact (ISO-CD-11227).

[6] K. Sugahara, K. Aso, Y. Akahoshi, T. Koura, T. Narumi, Intact measurement of fragments in ejecta due to hypervelocity impact, Proc. 60th Int. Astronautical Cong., (2009) IAC-09-A6.3.06.

[7] J.M. Siguier, J.C. Mandeville, Test procedures to evaluate spacecraft materials ejecta upon hypervelocity impact, Proc. IMechE G 221 (2007) 969–974.
[8] T. Michikami, K. Moriguchi, S. Hasegawa and A. Fujiwara, Ejecta velocity distribution for impact cratering experiments on porous and low strength targets, Planetary and Space Science 55 (2007) pp. 70-88 .
[9] S. Takasawa, A. M. Nakamura, T. Kadono, M. Arakawa, K. Dohi, S. Ohno, Y. Seto, M. Maeda, K. Shigemori, Y. Hironaka, T. Sakaiya, T. Sano, T. Watari, K. Sangen and T. Takeuchi, Ejecta size distribution from hypervelocity impact cratering of planetary materials: Implication for dust production process of impact origin, European Planetary Science Congress 2010 Abstracts, 5 (2010), EPSC2010-179.
[10] D.E. Grady and M.E. Kipp, Impact failure and fragmentation properties of metals, Sandia Report SAND 98-0387, (1998).
[11] A.J. Piekutowski, Formation and description of debris clouds produced by hypervelocity impact, NASA Contractor Report 4707, (1996).
[12] L.J. DeChant, Validation of a computational implementation of the Grady-Kipp dynamic fragmentation theory for thin metal plate impacts using an analytical strain-rate model and hydrodynamic analogues, Mech Mater 37 (2005), pp. 83–94.
[13] F.E. Allison, K.R. Becker, R. Vitali, Effects of target temperature on hypervelocity cratering, In Proceedings of fourth symposium on hypervelocity impact, Eglin Air Forth Base, FL, 1960. pp 1-12: CD Compilation of Original Hypervelocity Impact Symposia, Southwest Research Institute, San Antonio, TX, May 2008.
[14] B.M. Corbett, Numerical simulations of target hole diameters for hypervelocity impacts into elevated and room temperature bumpers, Int. J. Impact Eng. 33 (2006), pp. 431–440.
[15] B. M. Corbett, Selecting a best-fit temperature-dependent regression model for thin target HVI data, Int. J. Impact Eng. 35 (2008), pp. 1672–1677.
[16] D. Numata, K. Ohtani, M. Anyoji, K. Takayama, M. Sun, Experimental study of hypervelocity impacts at low temperatures, Shock Waves 18 (2008), pp.169-183.
[17] D. Numata, K. Ohtani, M. Anyoji, K. Takayama, K. Togami, M. Sun, HVI tests on CFRP laminates at low temperature, Int J Impact Eng 35 (2008), pp.1695-1701.
[18] A. Francesconi, D. Pavarina, C. Giacomuzzoa and F. Angrillia, Impact experiments on low-temperature bumpers, Int J Impact Eng 33 (2006), pp. 264-272.
[19] B.K. Wells, Hypervelocity impact tests on coated thermoplastic films at cryogenic and elevated temperatures, Int J Impact Eng 33 (2006), pp. 855-861.
[20] Structures and properties of aluminum, Japan Institute of Light Metals ed., 1991 478 (in Japanese).
[21] K.B. Hayashida and J.H. Robinson, Single wall penetration equations, NASA TM-103565 (1991) pp. 3-5.
[22] A. J. Watts and D. Atkinson, Dimensional scaling for impact cratering and perforation, Int J Impact Eng 17 (1995) pp. 925-935.
[23] A. Watts, D. Atkinson and S. Rieco. Dimensional scaling for impact cratering and perforation, NASA CR -188259 (1993).

[24] S. Lieblein, N, Clough and A.R. McMillan, Hypervelocity impact damage characteristics in armored space radiator tubes, NASA TN-D-2472 (1964) pp. 10-11.
[25] R. Piacesi, R.H. Waser and V.C.D. Dawson, Temperature-yield strength correlation of the crater size produced in aluminum by the hypervelocity impact of aluminum spheres, NOLTR 63–142 (1964) pp. 1-3.
[26] F.E. Allison, K.R. Becker and R. Vitali, Effects of target temperature on hypervelocity cratering, Proceedings of 4th symposium on hypervelocity impact, (1960) pp. 1-12.
[27] B.A. Myers, W.P. Schonberg and J.E. Williamsen, Temperature effects on bumper hole diameters for impact velocities from 2 to 7 km/sec. Int J Impact Eng, 29(1–10) (2003) pp. 487–95.

Table 1 Material properties of aluminum alloy 6061-T6

Temperature [°C]	+205	+25	-196
Elastic modulus [GPa]	77	70	63
Tensile strength [MPa]	130	310	415
Yield stress [MPa]	105	275	325
Elongation at break [%]	28	17	22
Temperature [°C]	+200	+25	-150
Vickers hardness	100	110	128

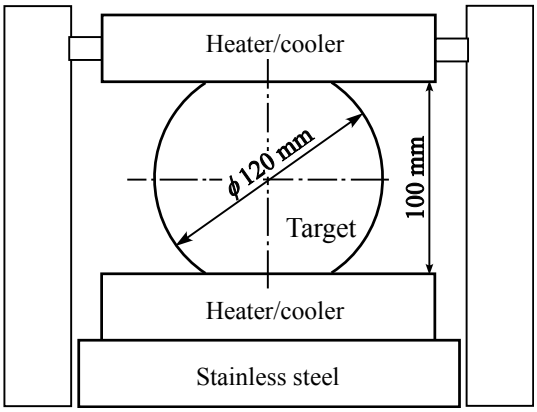

Figure 1 Shape and size of targets

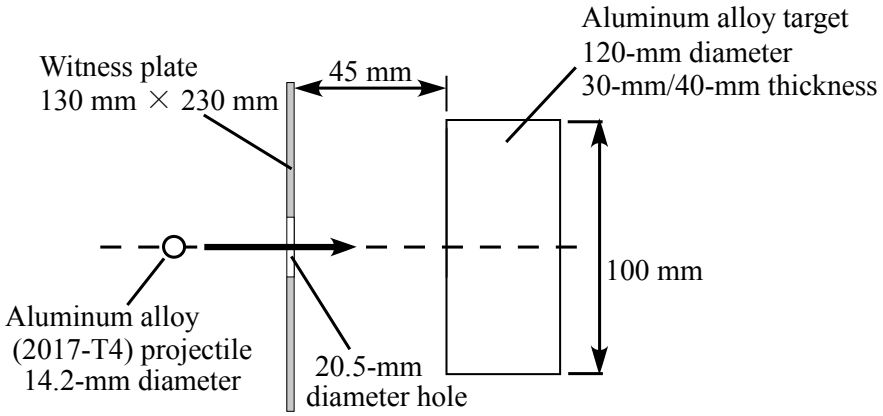

Fig. 2. Experimental setup for hypervelocity impact

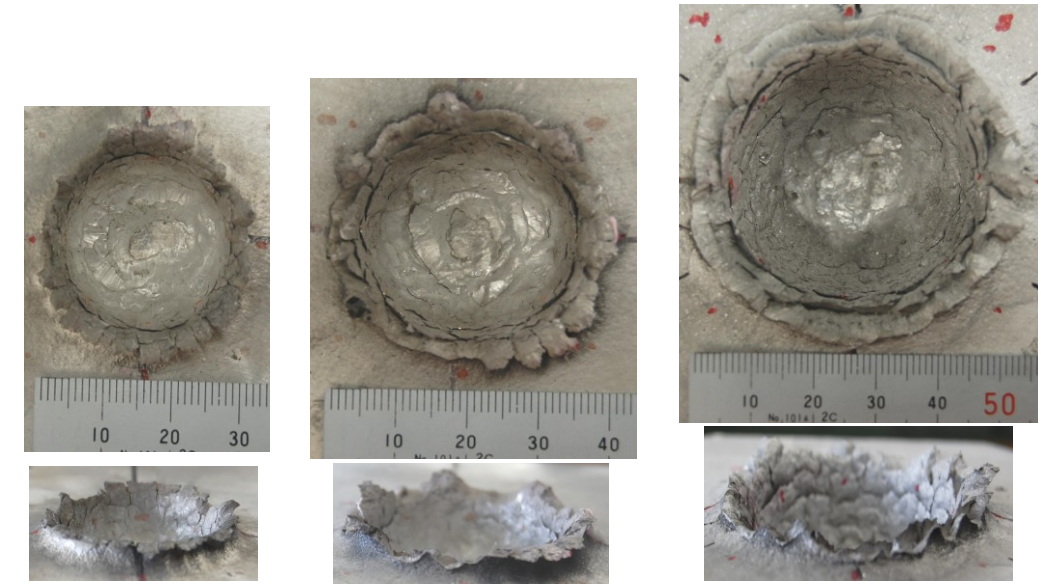

(a) +210°C, 1.37 km/s (b) +202°C, 2.14 km/s (c) +206°C, 3.47 km/s

Figure 3 Observation of craters; Effect of impact velocity at high temperatures

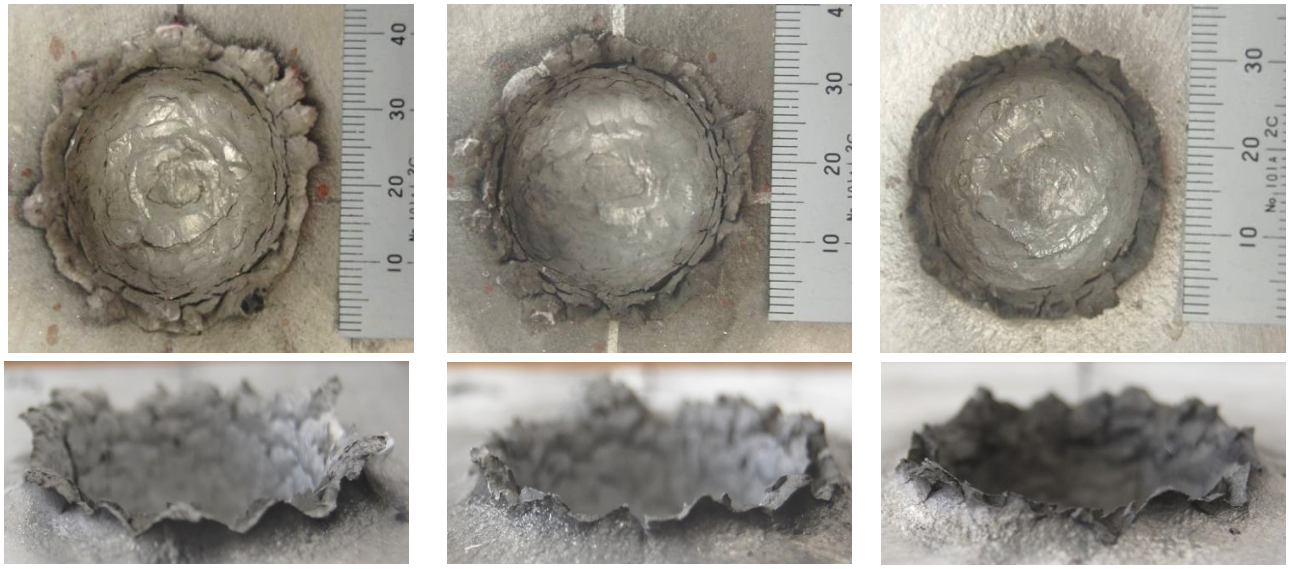

(a) +197°C, 2.67 km/s (b) +16°C, 2.63 km/s (c) -157°C, 2.67 km/s

Figure 4 Effect of temperature on crater shape (impact velocity: approximately 2.5 km/s)

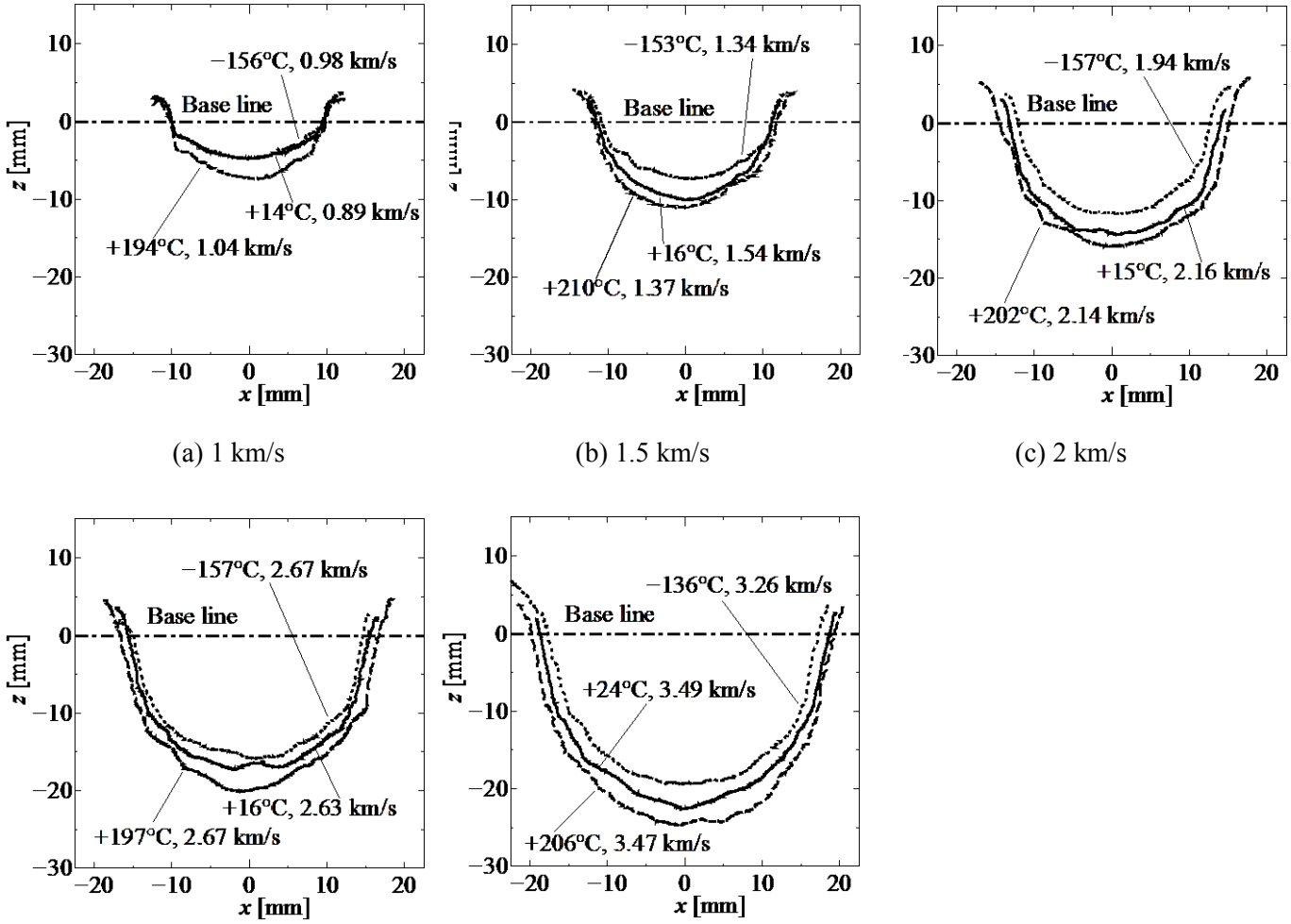

(a) 1 km/s (b) 1.5 km/s (c) 2 km/s

(d) 2.5 km/s (e) 3.5 km/s

Figure 5 Effect of temperature on crater shapes

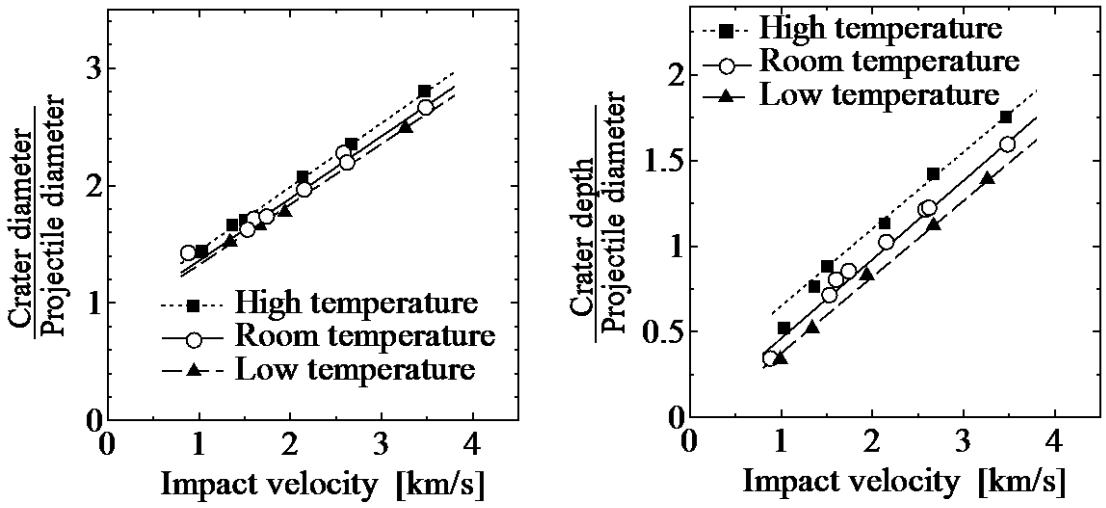

(a) Crater diameter

(b) Crater depth

Figure 6 Variation in crater diameter and depth with impact velocity

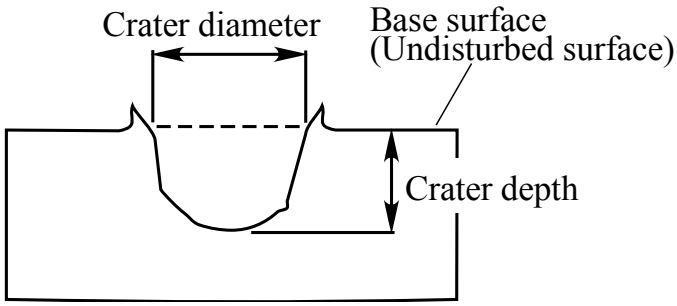

Figure 7 Definition of crater diameter and crater depth

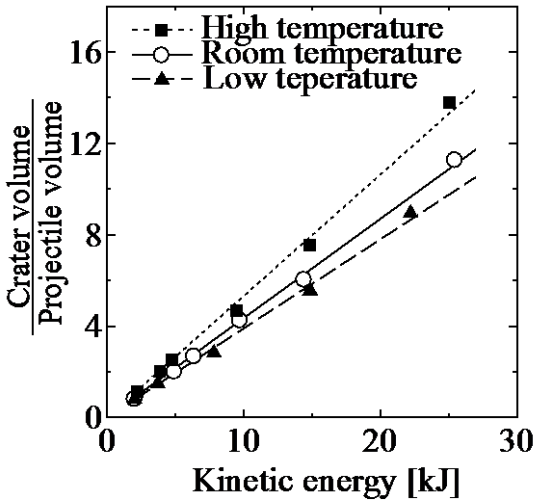

Figure 8 Variation in crater volume with impact velocity

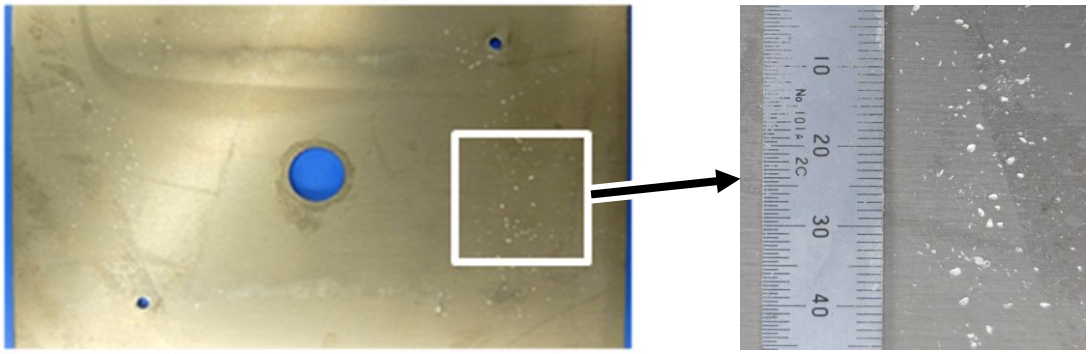

(a) +194°C, 1.04 km/s

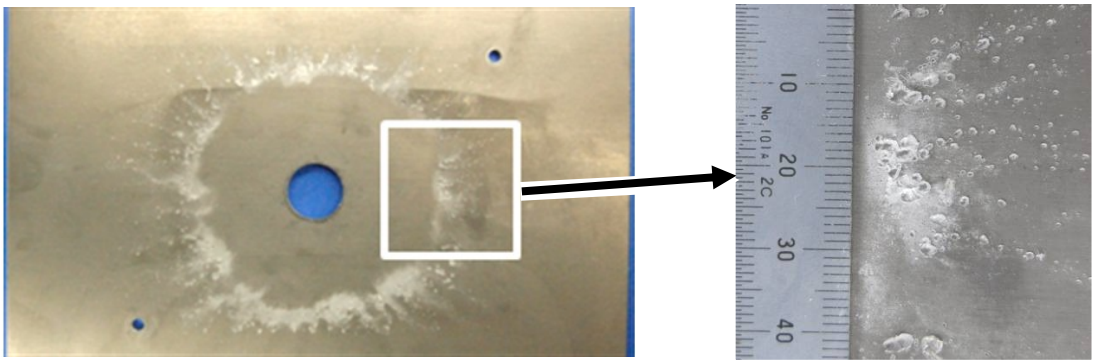

(b) +202°C, 2.14 km/s

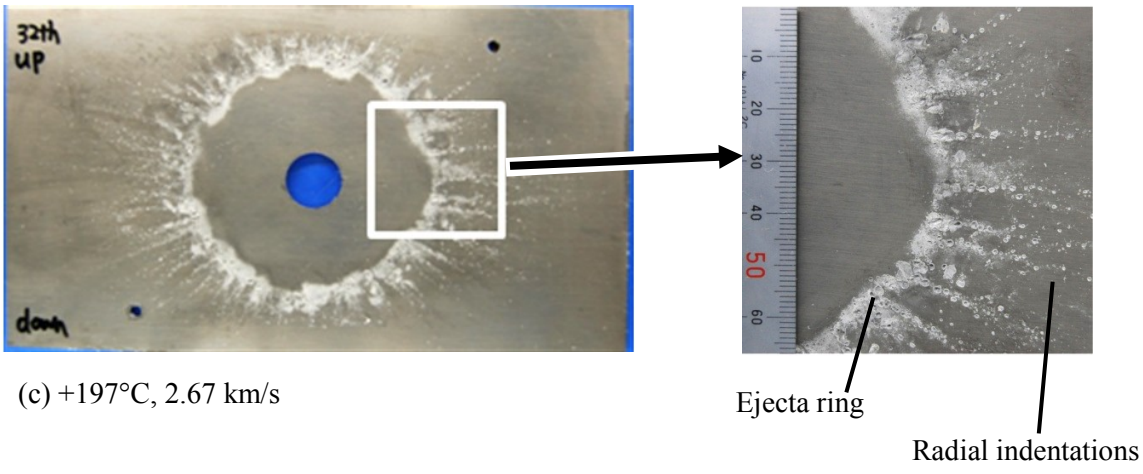

(c) +197°C, 2.67 km/s

Figure 9 Observation of indentation on witness plates; Effect of impact velocity at high temperature

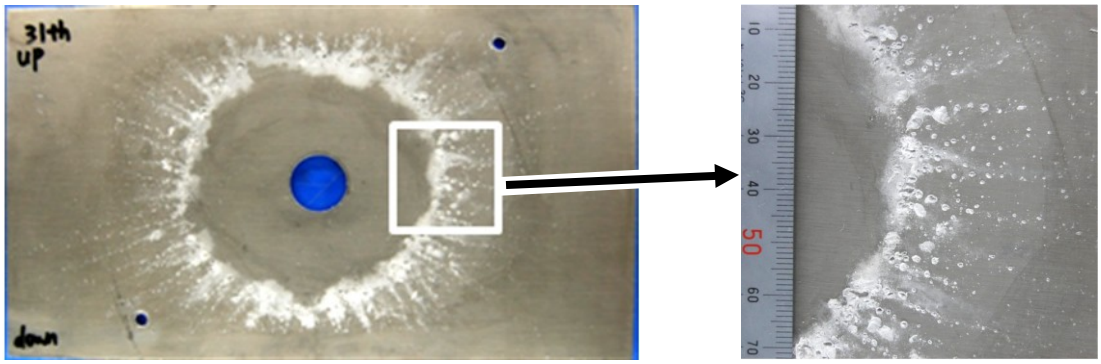

(a) +16°C, 2.63 km/s

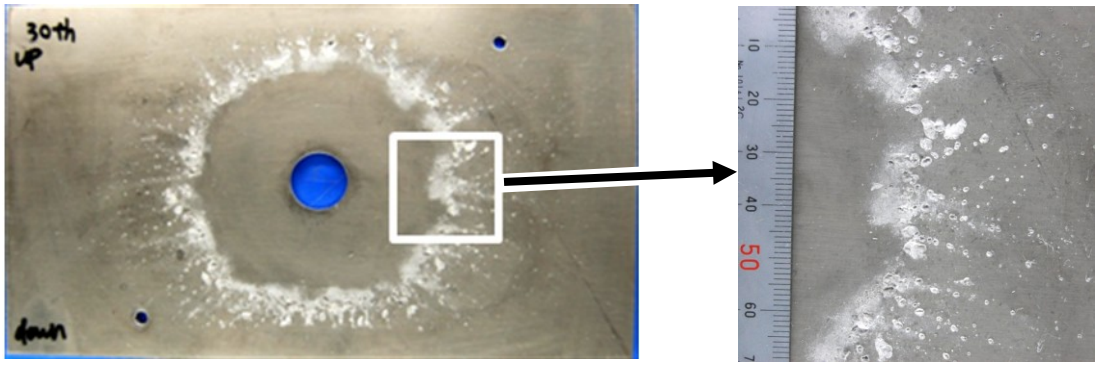

(b) -153°C, 2.67 km/s

Figure 10 Observation of indentation on witness plates (impact velocity: approximately 2.5 km/s)

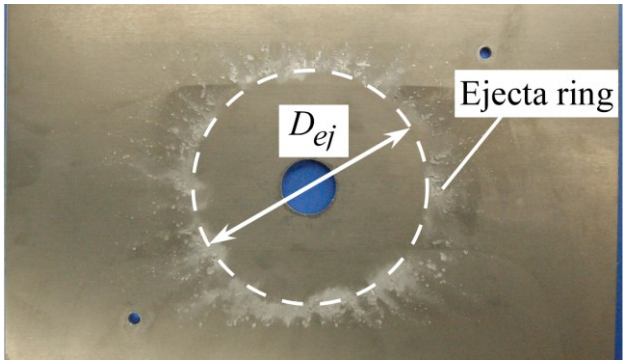

XXXXX

Figure 11 Definition of inner diameter of ejecta ring

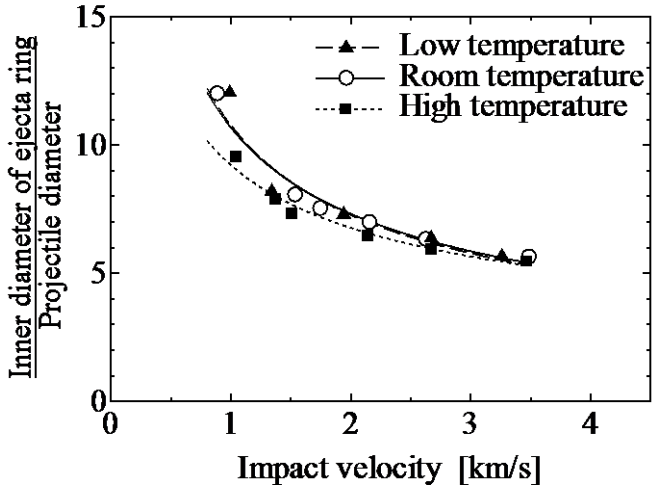

Figure 12 Impact velocity dependency of inner diameter of ejecta ring

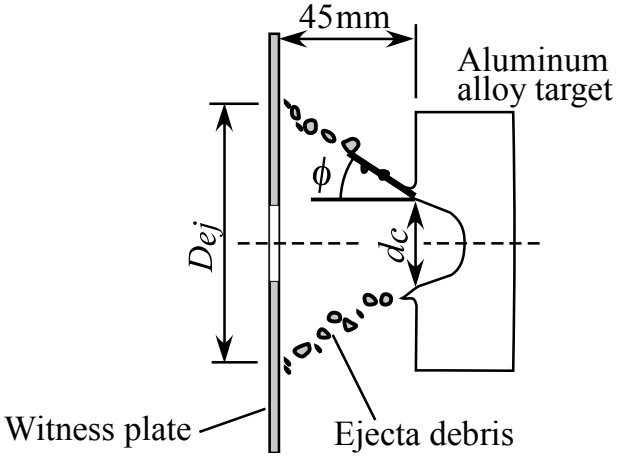

Figure 13 definition of scatter angle

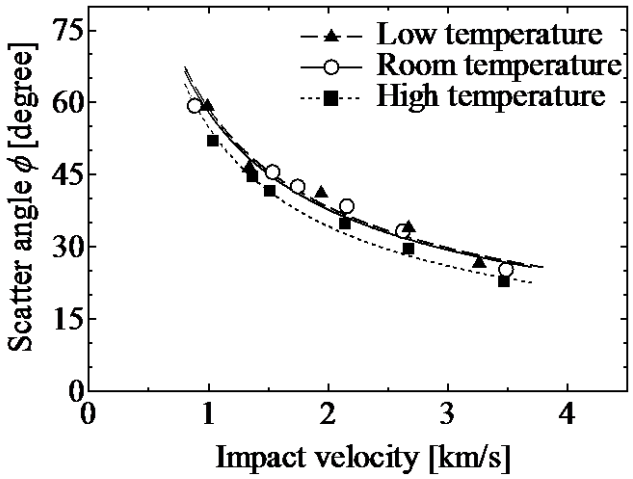

Figure 14 Impact velocity dependency of scatter angle

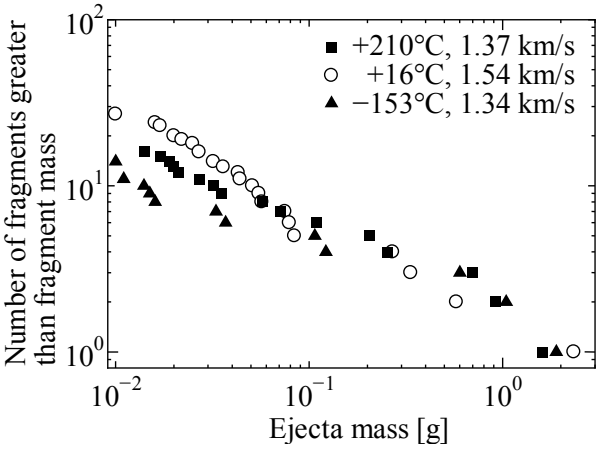

(a) 1.5 km/s

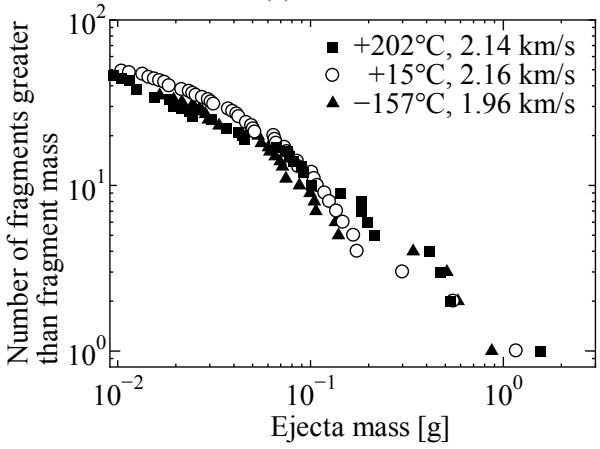

(b) 2.0 km/s

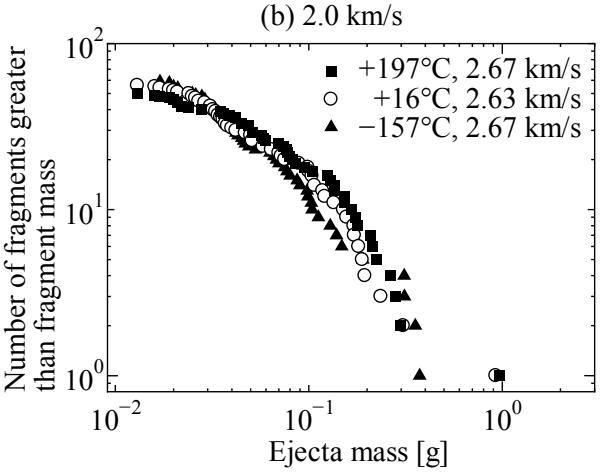

(c) 2.5 km/s

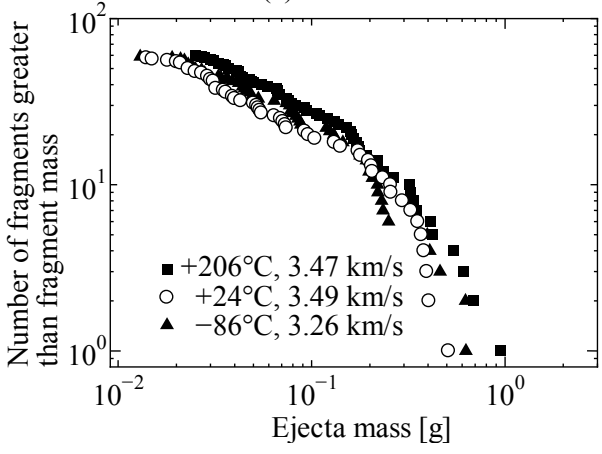

(d) 3.5 km/s

Figure 16 Effect of temperature on ejecta fragment mass

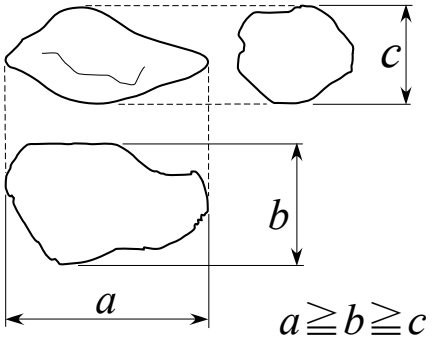

Figure 17 Definition of ejecta fragment size

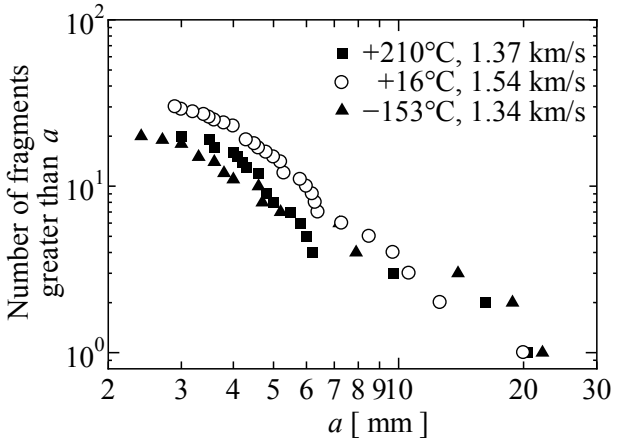

(a) 1.5 km/s

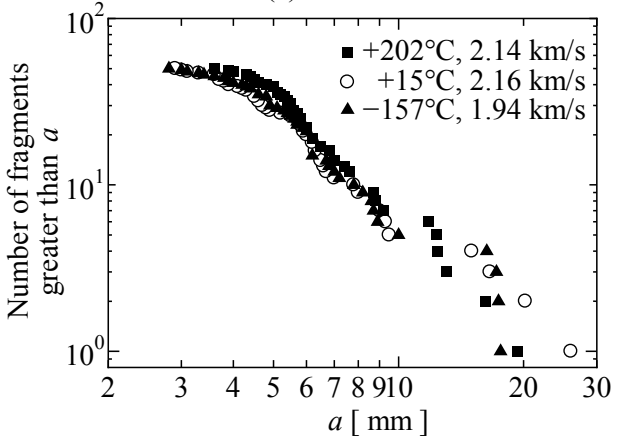

(b) 2.0 km/s

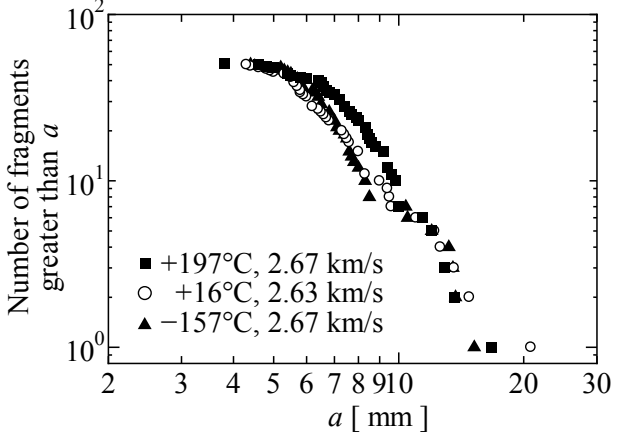

(c) 2.5 km/s

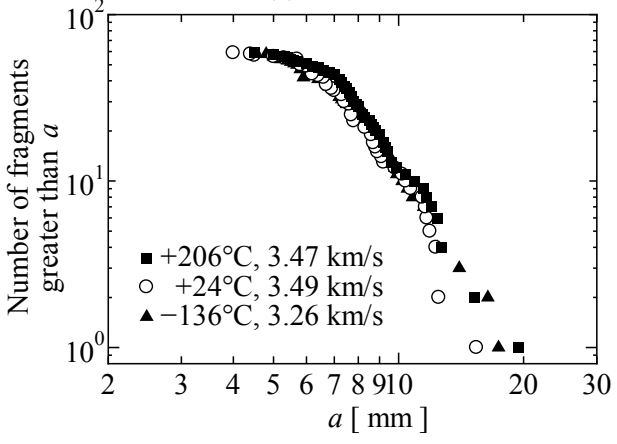

(d) 3.5 km/s

Figure 18 Effect of temperature on ejecta fragment length, *a*

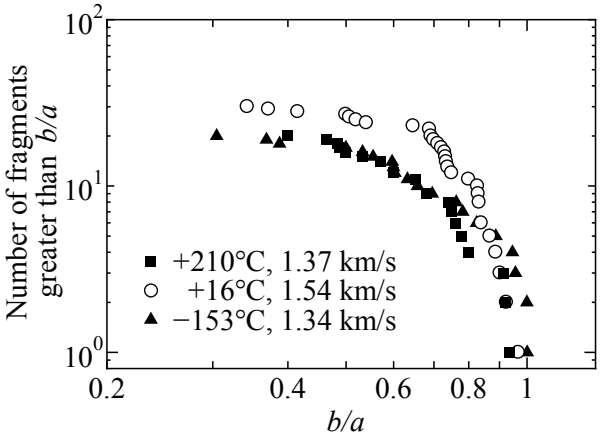

(a) 1.5 km/s

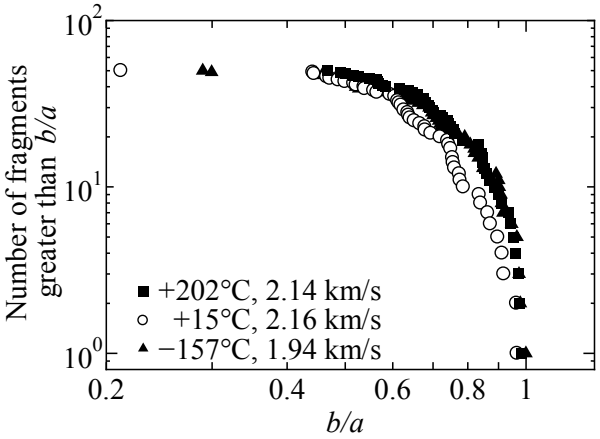

b) 2.0 km/s

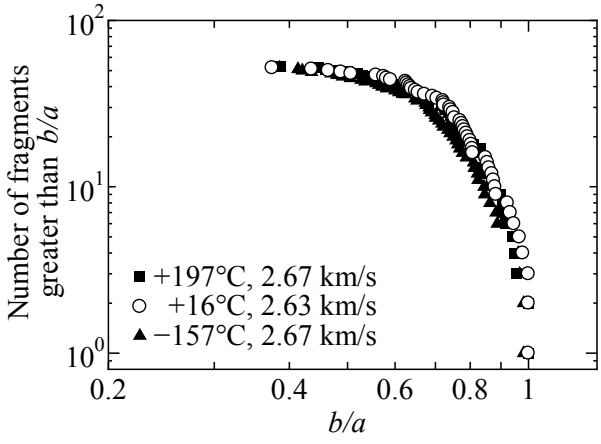

(c) 2.5 km/s

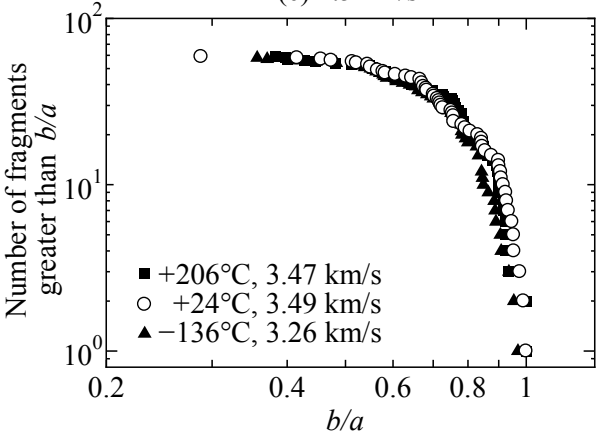

(d) 3.5 km/s

Figure 19 Axial ratio of ejecta fragments, *b*/*a*

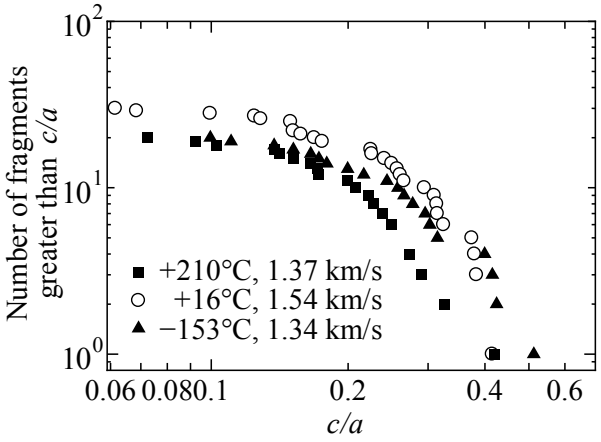

(a) 1.5 km/s

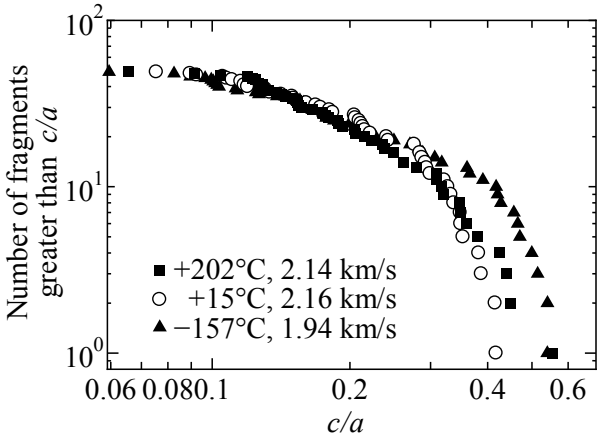

(b) 2.0 km/s

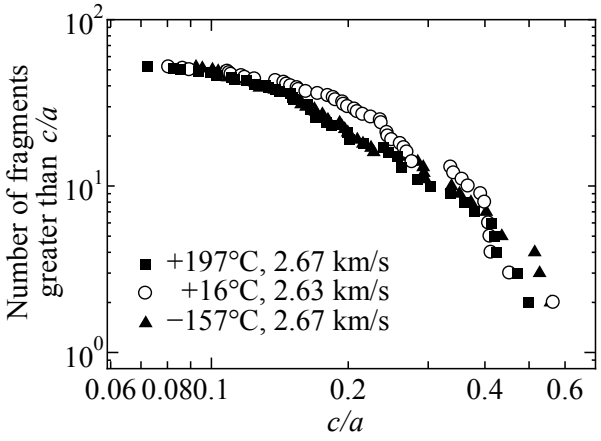

(c) 2.5 km/s

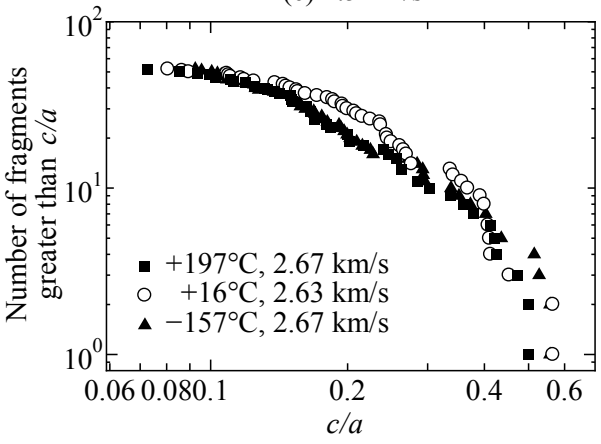

(d) 3.5 km/s

Figure 20 Axial ratio of ejecta fragments, *c*/*a*